Time-resolved molecular characterization of limonene/ozone aerosol using high-resolution electrospray ionization mass spectrometry†

Adam P. Bateman,[a] Sergey A. Nizkorodov,*[a] Julia Laskin[b] and Alexander Laskin[c]

Received 2nd April 2009, Accepted 17th June 2009
First published as an Advance Article on the web 27th July 2009
DOI: 10.1039/b905288g

Molecular composition of limonene/O_3 secondary organic aerosol (SOA) was investigated using high-resolution electrospray ionization mass spectrometry (HR-ESI-MS) as a function of reaction time. SOA was generated by ozonation of D-limonene in a reaction chamber and sampled at different time intervals using a cascade impactor. The SOA samples were extracted into acetonitrile and analyzed using a HR-ESI-MS instrument with a resolving power of 100 000 ($m/\Delta m$). The resulting mass spectra provided detailed information about the extent of oxidation inferred from the O : C ratios, double bond equivalency (DBE) factors, and aromaticity index (AI) values in hundreds of identified individual SOA species. The chemical composition of SOA was approximately the same for all size-fractionated samples studied in this experiment (0.05 to 0.5 μm range). The SOA constituents quickly reached an average O : C ratio of 0.43, which grew to 0.46 after one hour of additional oxidation of particles by the excess ozone. The dominant mechanism of oligomerization, inferred from high resolution ESI-MS data, was reaction between Criegee intermediates and stable first-generation products of limonene ozonolysis. Although the SOA composition was dominated by various oxidized aliphatic compounds, a small fraction of products appeared to contain aromatic rings. SOA generation was also studied in the presence of UV radiation and at elevated relative humidity (RH). The presence of UV radiation had a negligible effect on the SOA composition. The presence of water vapor resulted in a slight redistribution of peak intensities in the mass spectrum likely arising from hydration of certain SOA constituents. The data are consistent with fast production of the first-generation SOA constituents, including oligomers, followed by very slow aging processes that have a relatively small effect on the average molecular composition on the timescale of our experiments.

Introduction

Ozone-initiated oxidation of D-limonene, one of the most common biogenic monoterpenes,[1] makes a significant contribution to the atmospheric secondary organic aerosol (SOA) budget.[2–4] The chemical composition of limonene/O_3 SOA is known to be very complex, even for SOA prepared in carefully controlled smog chamber experiments.[5–12] Various chemical and photochemical aging processes following the initial SOA growth can further multiply the number of chemically distinct SOA constituents.[13–16] In an attempt to cope with this bewildering chemical complexity, scientists have recently examined chemical composition of limonene/O_3 and α-pinene/O_3 SOA with high-resolution electrospray ionization mass spectrometry (HR-ESI-MS).[17–19] The main advantage of this technique is that it provides information about hundreds of individual SOA species and their elemental formulae can be unambiguously assigned based on accurately measured m/z values of the corresponding mass spectral peaks. The HR-MS methods are by no means limited to the analysis of laboratory-generated SOA; they have been successfully applied to molecular characterization of water-soluble components in biomass-burning aerosols[20,21] and rural particulate matter.[22]

The initial steps for oxidation of limonene by ozone leading to SOA are relatively well known.[23] However, aging reactions occurring after the SOA formation, including reactive uptake of gas-phase species and reactions of SOA constituents with themselves, with water vapor, and possible effects of ultraviolet radiation are not well understood. The main objective of this study is to examine the variance of SOA chemical composition with particle size, reaction time, humidity, and UV radiation using HR-ESI-MS methods of analysis. This work extends on our previous study,[18] which probed limonene/O_3 aerosol under a single set of reaction conditions,

[a] *Department of Chemistry, University of California, Irvine, Irvine, California 92697, USA. E-mail: nizkorod@uci.edu; Fax: +1-949-824-8571; Tel: +1-949-824-1262*
[b] *Chemical and Materials Sciences Division, Pacific Northwest National Laboratory, Richland, Washington 99352, USA*
[c] *Environmental Molecular Sciences Laboratory, Pacific Northwest National Laboratory, Richland, Washington 99352, USA*

† Electronic supplementary information (ESI) available: Sample SMPS data taken during SOA preparation (Fig. S1); sample mass spectra of limonene/O_3 SOA (Fig. S2); a two-dimensional version of Van Krevelen diagram shown in Fig. 1 (Fig. S3); structures of selected first-generation products of limonene ozonolysis (Fig. S4); particle-size resolved Van Krevelen diagram (Fig. S5); summary of peaks excluded and assigned during peak analysis (Table S1). In addition, a table of all assigned peaks in the positive ion mode mass spectrum of limonene/O_3 SOA is provided as a separate text file. See DOI: 10.1039/b905288g

by examining the evolution of SOA chemical composition as a function of particle size and reaction time.

Experimental

Limonene/O_3 SOA was generated from the reaction of D-limonene vapor and O_3 in an inflatable Teflon FEP reaction chamber. The chamber was purged several times and filled with zero air (99.998%) to ~400 L. Ozone was introduced by adding pure oxygen through a commercial ozone generator (Pacific Ozone, Model L11/R-LAB111) and turning the generator on for several seconds. The concentration of ozone was adjusted to approximately 1 ppm, as measured with a commercial ozone monitor (Thermo Electron UV photometric O_3 analyzer). After the ozone concentration stabilized, a 10 μL mixture containing 25 vol.% D-limonene (98% purity, Acros Organics) and 75 vol.% cyclohexane (HPLC grade) was injected with a gas-tight syringe through a septum to achieve an initial limonene mixing ratio on the order of 1 ppm. We have previously shown that the presence of OH scavenger does not have a significant effect on the limonene/O_3 SOA mass spectrum,[18] therefore we have not attempted experiments with different amounts of added cyclohexane. However, it is certainly possible that a fraction of SOA compounds may originate from OH-initiated oxidation of limonene.[24] Following the injection, limonene and cyclohexane quickly evaporated and the resulting gas-phase mixture reacted to produce particles. No mixing was used in the chamber in order to minimize wall losses.

Most experiments were conducted in dark and dry conditions. Additional experiments were conducted in humidified air generated by the bubbling of zero air through two bubblers filled with nanopure water. Another set of experiments was conducted in the presence of UV radiation produced by 8 UV-A lamps (Sylvania, Inc., model F20T12/350BL) and 6 UV-B lamps (Light Sources, Inc., model FS20T12/UVB-BP-emission centered at 310 nm). The lamps were mounted on both sides of the Teflon reaction chamber, approximately 10 cm away from the chamber walls. Operation of these lamps resulted in a 3–5 °C temperature increase in the chamber relative to the room temperature. The UV radiation from the lamps did not decompose ozone in the chamber to any measurable extent but it could potentially photolyze peroxides and aldehydes in SOA particles. The lamps were therefore used to simulate ozone and limonene reaction under sunlight (daytime) conditions. The particle concentration in the chamber was measured with a scanning mobility particle sizer (SMPS), which consisted of a differential mobility analyzer (DMA) platform (TSI, model 3080), DMA column (TSI, model 3081) and condensation particle counter (TSI, model 3025A). Representative particle size and number concentration data obtained from the SMPS system are included in Fig. S1 of the ESI section. The geometric mean particle diameter typically reached ~0.3 μm after thirty minutes of reaction and continued to increase slowly after that.

A micro-orifice uniform-deposition impactor (MOUDI, MSP Corp., model 110-R) was used to collect size-fractionated samples of SOA. Aluminum foil substrates were used to collect the samples on the lowest five stages: 6 through 10 (cut-off sizes of D_{50} = 0.56, 0.32, 0.18, 0.10, and 0.056 μm, respectively). Filmed microscopy grids (Carbon Type-B, 400 mesh copper grids, Ted Pella Inc.) were mounted on the aluminum foils to collect particle samples for computer controlled scanning electron microscopy (CCSEM) analysis. CCSEM analysis of SOA particles morphology and sizes was performed using a FEG XL30 digital scanning electron microscope (FEI, Inc.); specific details of the analysis are provided elsewhere.[25] The SOA samples were collected at a flow rate of 30 L min^{-1}. The collection time varied depending on the intended analysis: 30 s–2 min for CCSEM; 2–4 min for HR-ESI-MS. Two sets of samples at different times were collected in most experiments: 10 and 90 min after adding limonene to the chamber. As the chamber volume was ~400 L, collecting more than two sets of samples per experiment was not feasible. A significant amount of particles was reproducibly collected on stages 7–10 (0.32–0.056 μm). Stage 6 (1.0–0.56 μm) collected almost an order of magnitude less material than stages 7–10 resulting in inferior signal-to-noise ratio in mass spectra of stage 6 samples. Stages 1–5 (>1.0 μm) collected no visible amount of particles, and were not used for the ESI-MS analysis. After the aluminum foils were removed from MOUDI, the microscopy grid substrates were detached and used for SEM imaging. The remaining foils were then cut into small pieces, sonicated for 20 min in 1 mL of acetonitrile, and filtered with syringe filters (glass microfiber filter, 0.7 μm pore size—Whatman, Inc.) for the ESI-MS analysis. Blank samples were also prepared and analyzed following all of the steps above except for the SOA collection.

A modified 3-Stage Davis Rotating-drum Uniform-size-cut Monitoring (DRUM) impactor[26] (UC Davis, CA) was used to collect particles as a function of the reaction time. This instrument collected particles by impaction on three rotating drums. Each drum contained a strip of collecting substrate, either Teflon or Aluminum foil, attached around the circumference of the drum. The drums were controlled by a stepper motor, which advanced the strip by 5 mm every 4 min. This resulted in SOA material collected into ~2 mm spots, each spot corresponding to a specific 4-min reaction time interval. The aerodynamic size ranges were 1.2–2.5 μm (drum A), 0.34–1.2 μm (drum B), and 0.07–0.34 μm (drum C). The vast majority of particles were collected on drum C, therefore, only samples from drum C were used for ESI-MS analysis. Typically, 16–20 samples were collected in one experiment with 4 min time resolution. After the experiment, the relevant segments were cut out from the strip substrate, placed into labeled vials, and sonicated for twenty minutes in 1 mL of acetonitrile. The samples collected on Teflon strips did not need additional filtration, as there was no significant substrate degradation during sonication. Aluminum foil substrates partly disintegrated during sonication, requiring filtration with a syringe filter.

Solvent extracted samples were analyzed using a Finnigan LTQ (linear ion trap)-Orbitrap^{TM} hybrid mass spectrometer (Thermo Electron Corporation, Inc.) with a modified ESI source. Samples were injected through a pulled fused silica capillary tip (50 μm id) at a flow rate ranging from

0.6–1.0 μL min^{-1}. The resolving power was set to either 60 000 or 100 000 ($m/\Delta m$ at m/z 400) in both positive and negative ionization modes. Calibration was frequently verified using a standard solution of caffeine, MRFA, and Ultramark 1621.

Data analysis and results

1 HR-MS data analysis and visualization tools

Analysis of the HR-MS data benefit from a number of advanced data processing and visualization tools, such-as van Krevelen (VK) diagrams,[27,28] Kendrick plots,[29] double bond equivalency index (DBE),[30,31] and aromaticity index (AI).[32] These techniques greatly aid in the molecular assignment of the many peaks in each mass spectra which in turn allows assessment of the chemical properties and composition of complex SOA molecules. The most commonly used variation of VK diagrams plots the O : C ratios on the x-axis and the H : C ratios on the y-axis, thus classifying each molecule by its individual O : C and H : C ratios. Kendrick plots make it possible to easily recognize homologous families of molecules built by repeated addition of structural units (*e.g.*, CH_2 or O). DBE is a convenient measure of the number of rings and unsaturated bonds in a molecule.

All SOA constituents examined in this work are closed-shell molecules, $C_cO_oH_h$, containing c carbon atoms, h hydrogen atoms, o oxygen atoms, and no other elements. Triple carbon–carbon bond are quite unlikely to occur in limonene/O_3 SOA molecules. With these constraints, the DBE value,

$$\mathrm{DBE} = 1 - \frac{h}{2} + c \qquad (1)$$

should be equal to the total number of C=C bonds, C=O bonds, and rings in the molecule.

The aromaticity index is a useful metric of the extent of aromaticity. For a molecule that contains only carbon, oxygen, and hydrogen atoms, AI is calculated as[32]

$$\mathrm{AI} = \frac{1 + c - o - \frac{h}{2}}{c - o} (= 0 \text{ if negative}) \qquad (2)$$

Positive values of AI can result from presence of multiple C=C (but not C=O) double bonds or aromatic rings in such molecules. For example, benzoic acid ($C_7H_6O_2$) has an AI value of 0.6, which is smaller than that of benzene (AI = 0.67) despite having a C=O bond in its structure. In general, the AI values in excess of 0.5 indicate the presence of isolated aromatic rings in the molecule, while values in excess of 0.67 are characteristic of polyaromatic compounds with fused rings.[31] One has to keep in mind that the value of AI > 0.5 does not necessarily provide a proof of aromaticity as highly conjugated aliphatic systems also have reasonably large AI values. For example, the AI of butadiene (C_4H_6), which is not an aromatic molecule, is 0.5.

Many field and laboratory studies rely on measuring the organic carbon mass (OC) of collected particulate matter. The total organic mass (OM) is then estimated by multiplying the OC mass by a constant conversion factor, which was historically set at 1.4. More recently proposed literature values of OM : OC for urban and non-urban organic aerosol are, 1.6 ± 0.2 and 2.1 ± 0.2, respectively.[32,33] The OM : OC conversion factor is a strong function of the organic oxygen content of the aerosol, which is difficult to quantify using traditional analytical techniques. High-resolution mass-spectrometry could provide a valuable complementary method for measurements of the OM : OC ratio.[34]

To illustrate the approach used in this work, consider limonene/O_3 SOA sample that has i different chemical species with molar fractions x_i and individual molecular formulas $C_{c_i}O_{o_i}H_{h_i}$. The ratio of the total number of organic oxygen atoms to that of organic carbon atoms is then:

$$\frac{N_\mathrm{O}}{N_\mathrm{C}} = \sum_i x_i o_i \Big/ \sum_i x_i c_i \qquad (3)$$

The ratio of the organic oxygen (OO) mass to the organic carbon (OC) mass in the sample can be obtained by scaling eqn (3) by the corresponding atomic weights.

$$\frac{\mathrm{OO}}{\mathrm{OC}} = \frac{16}{12} \sum_i x_i o_i \Big/ \sum_i x_i c_i \qquad (4)$$

The OM : OC ratio can be calculated in a similar way

$$\frac{\mathrm{OM}}{\mathrm{OC}} = 1 + \frac{16}{12} \sum_i x_i o_i \Big/ \sum_i x_i c_i + \frac{1}{12} \sum_i x_i h_i \Big/ \sum_i x_i c_i \qquad (5)$$

The average O : C ratio can alternatively be calculated in a molecule-by-molecule fashion:

$$\langle \mathrm{O} : \mathrm{C} \rangle = \sum_i x_i \frac{o_i}{c_i} \qquad (6)$$

Note that the quantity obtained in eqn (6) is not the same as the one in eqn (3), and it cannot be easily related to the OO : OC mass ratio. The main advantage of eqn (6) is that it is more closely related to the van Krevelen representation of mass spectra as discussed below. For all limonene/O_3 SOA samples discussed here, eqn (3) and eqn (6), gave nearly identical results.

For the ESI-MS analysis, the SOA sample is dissolved in an appropriate solvent. The ESI-MS instrument measures ion counts, which, for a sufficiently dilute solution, should be directly proportional to the molar fractions of respective organic molecules.

$$\mathrm{Intensity}_i = \mathrm{Sensitivity}_i \times x_i \qquad (7)$$

If all the sensitivity factors are the same, the molar fractions in eqns (3)–(6) can be replaced with the corresponding normalized peak intensities in the mass spectrum. For example, the average O : C ratio is obtained as follows:

$$\langle \mathrm{O} : \mathrm{C} \rangle = \sum_i \mathrm{Intensity}_i \frac{o_i}{c_i} \Big/ \sum_i \mathrm{Intensity}_i \qquad (8)$$

Similar equations can be written for the average H : C ratio, and the average DBE value:

$$\langle \mathrm{H:C} \rangle = \sum_i \mathrm{Intensity}_i \frac{h_i}{c_i} \Big/ \sum_i \mathrm{Intensity}_i \quad (9)$$

$$\langle \mathrm{DBE} \rangle = \sum_i \mathrm{Intensity}_i (\mathrm{DBE})_i \Big/ \sum_i \mathrm{Intensity}_i \quad (10)$$

Several recent studies estimated the OM : OC ratio in complex mixtures of organics assuming equal ionization efficiencies for various compounds without systematically testing the validity of this assumption.[35,36] ESI response is a complex function of the solution composition, concentration of analytes and instrumental factors.[37,38] It is well-known that ESI is sensitive towards polar organic molecules containing basic or acidic groups and nonpolar molecules that can readily form adducts with electrolyte ions in solution. Other nonpolar molecules such as aliphatic hydrocarbons, polycyclic aromatic hydrocarbons or cholesterol are usually not observed in ESI spectra. It has been demonstrated that surface active molecules are most responsive to ESI analysis suggesting that ESI is most sensitive to molecules that have significant nonpolar regions and contain ionizable functional groups, while highly oxygenated soluble organic molecules may be not well represented in ESI/MS spectra.[37,39] Because all first-generation products of limonene ozonolysis contain at least one functional group that is capable of ionization in an ESI source and retain the surface active hydrocarbon backbone of the precursor molecule, it is reasonable to assume similar sensitivity of ESI-MS experiments to different ozonolysis products. In summary, one should treat the quantities calculated from eqns (8)–(10) as approximate but nonetheless very useful measures of the overall degree of oxidation of SOA constituents.

2 Data analysis

To process the large number of mass spectra recorded during this work, we have developed a number of batch processing and data analysis tools. For each spectrum, a list of peak positions and intensities was generated by Decon2LS program developed in the Pacific Northwest National Laboratory (http://ncrr.pnl.gov/software/). Only peaks with a signal-to-noise (S/N) of 3 and higher were included. The peak lists for all files in the same experimental batch, including blank samples, were sorted by a LabView 7.0 program to generate a master table of all observed peaks with a common m/z axis. Another LabView 7.0 program calculated the suggested $C_xH_yO_zNa^+$ and/or $C_xH_yO_zH^+$ assignments for every m/z value with relatively strict restrictions imposed on (typical values are given in parenthesis): the maximal number of atoms, ($c < 50$; $h < 100$; $o < 60$; number of sodium atoms, $Na = 0$ or 1); range of possible DBE values (−0.5 to 10.5); O : C values (0.05–1.3); H : C values (0.7–2.0); and m/z tolerance (<0.001). Half-integer values of DBE correspond to protonated, sodiated, or deprotonated ions if h in eqn (1) is taken to include both hydrogen and sodium atoms. DBE values for the corresponding neutrals are all integer numbers. Peaks with even nominal masses corresponding to molecules containing one ^{13}C atom and/or impurities were excluded. This initial set of assigned peaks was used to verify the accuracy of the calibration of the m/z axis; deviations between the exact m/z values and experimentally measured ones were typically within ±0.0005 m/z units over the 100–1000 m/z range. If systematic deviations in excess of this value were noticeable, the m/z axis was re-calibrated with respect to peaks, which were assigned with certainty. The following peaks were excluded: (i) peaks that were observed in blank samples; (ii) peaks that appeared in only a small fraction of SOA samples within a given batch; (iii) peaks that produced unrealistic values of mass defects, DBE, O : C ratio, and H : C ratio; (iv) peaks that could not be assigned to either $C_xH_yO_zNa^+$ and/or $C_xH_yO_zH^+$ ions within the specified m/z tolerance. The average number of the assigned peaks and the percentage of total ion current in each category above are included in Table S1 of the ESI.† The vast majority of the assigned peaks corresponded to sodiated molecules ($C_xH_yO_zNa^+$). Protonated molecules ($C_xH_yO_zH^+$) typically accounted for less than 10% of the peaks, and were always accompanied by the corresponding sodiated counterparts. After the peak assignment for a given batch of SOA samples was complete, we calculated O : C and H : C ratios, Kendrick mass defects, and DBE values *for the corresponding neutral species* (Na^+ and H^+ were subtracted from $C_xH_yO_zNa^+$ and $C_xH_yO_zH^+$ ions, respectively). All data discussed below correspond to *the neutral SOA constituents*.

3 Results

Our previous work presented positive and negative ion mode mass spectra of limonene/O_3 SOA generated under dry conditions, in dark, in pure oxygen, and with comparable (ppm level) initial concentrations of reagents.[18] Mass spectra and, as expected, the generated VK plots obtained in this work look very similar to those reported by Walser *et al.*[18] An example of a positive ion mode mass spectrum and VK diagram is provided in Fig. S2 and S3 of the ESI section,† respectively. We were able to observe and assign more peaks compared to our previous work.[18] However, the general features of the mass spectrum and VK diagrams are the same. The most recognizable feature of the mass spectrum is clustering of peaks into the monomeric range (<300 m/z), dimeric range (300–500 m/z), trimeric range (500–700 m/z), and tetrameric range (700–1000 m/z) corresponding to products containing one, two, three, and four oxygenated limonene units, respectively. Similar clustering of peaks in mass-spectra has been observed in previous publications on the chemical composition of monoterpene/O_3 SOA.[7,15,17,19,40–42]

The VK diagram shown in Fig. S3 of the ESI section† contains points with H : C ratios ranging from 1.1 to 1.8 and O : C ratios ranging from 0.2 to 0.7 for most compounds. Due to the chemical complexity of SOA, several different molecules often end up having the same H : C and O : C values in the VK diagram. It is therefore useful to use either DBE or molecular weight as an additional dimension for visualization of the HR-MS data. Fig. 1 shows the result of stretching the VK plot along the DBE dimension. Examination of this plot shows that the H : C ratios are anti-correlated with DBE

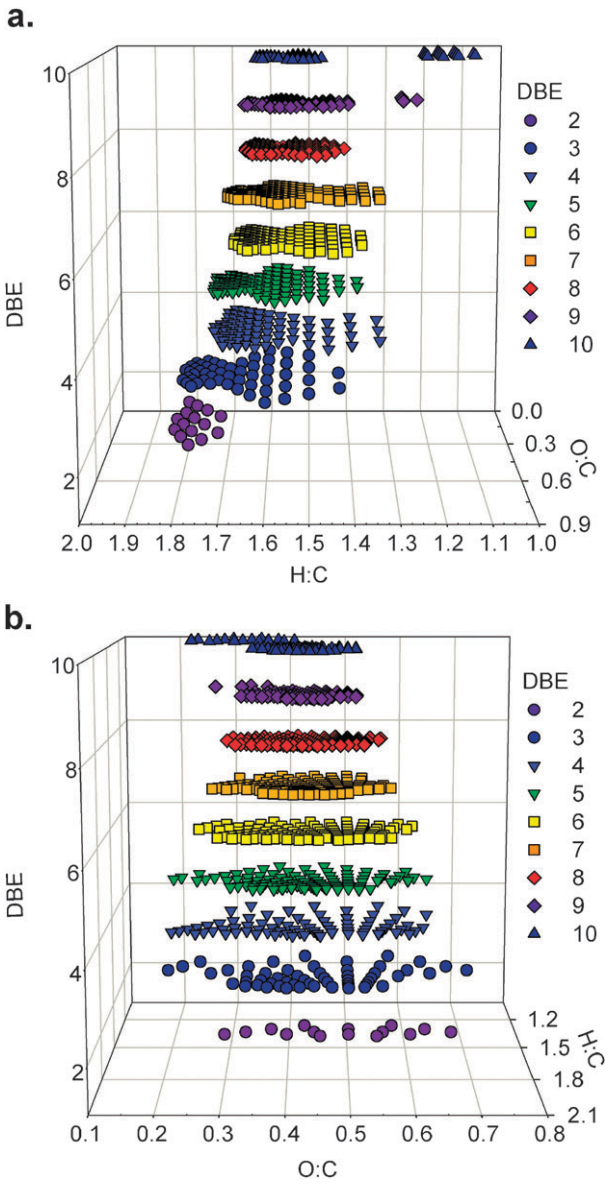

Fig. 1 An expansion of the van Krevelen (VK) plot along the DBE dimension for SOA from the dark reaction of limonene and ozone. The particles were collected using a DRUM impactor, extracted into acetonitrile, and immediately analyzed using ESI-MS. This sample corresponds to the first 4 min of reaction between ozone and limonene.

values, *i.e.* molecules with higher DBE tend to have lower average H : C ratios, as expected from eqn (1). The group of apparent outliers with very low H : C values (1.1–1.3) and high DBE values (9–10) is especially striking. No obvious trends with respect to DBE are observed for the O : C ratios.

The observed DBE values range from 2 to values exceeding 10, and appear to be positively correlated with the molecular weights of the SOA constituents (Fig. 2). For the majority of the molecules, DBE scales roughly linearly with molecular weight (one DBE unit per 100 g mol^{-1}). The outliers in this plot are the same ones that stand out in Fig. 1. They likely correspond to molecules formed by unique chemical processes; perhaps cyclization of the first generation SOA products leading to conjugated systems or even aromatic rings.

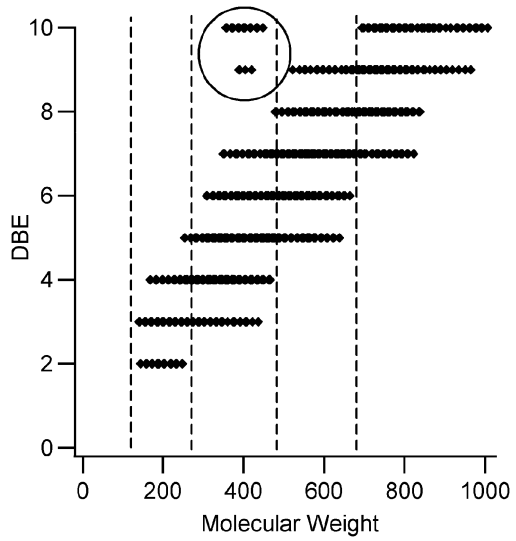

Fig. 2 DBE values plotted against molecular weights of SOA compounds for the sample in Fig. 1. Dashed lines separate different regions in the mass spectrum (monomers, dimers, trimers, tetramers). The circled group of points corresponds to molecules with positive values of AI.

Fig. 3 shows an SEM image of typical SOA particles collected on stage 7 of MOUDI and particles size distributions measured by CCSEM based on the equivalent circle diameters of two-dimensional projection areas. Close examination of the SEM image (Fig. 3a) reveals two interesting observations: (i) the distribution of the apparent particle sizes was quite broad; (ii) the apparent sizes of many collected particles significantly exceeded the expected size range for that MOUDI stage (0.56–0.32 μm for stage 7). Similar observations were made for particles collected on other MOUDI stages. Fig. 3b demonstrates that the normalized distributions of apparent particle sizes for all stages overlapped quite significantly. In contrast, collection of crystalline NaCl particles[43] and $CaCO_3$ particles[44] with the same MOUDI setup reproducibly resulted in much narrower size distributions. We believe that some of the amorphous, presumably jelly-like, SOA particles were flattened by the impaction onto the substrate, resulting in their two-dimensional projection areas larger than their original airborne size. An alternative possibility that SOA particles coagulated on the substrate after the impaction, similar to the coagulation of mercury droplets on a surface, is unlikely given that the size distribution of samples with much reduced total number of particles was also broad. As the particle impact velocity increases for smaller particles, the degree of particle flattening is larger for higher MOUDI stages (Fig. 3c). Despite the large width of the apparent size distribution, the average collected particle size did increase by a factor of four from stage 10 to stage 6 making it possible to investigate the effects of the average particle size on the SOA composition.

We compared the mass spectra of extracts from different MOUDI stages and collected at different times after mixing limonene and ozone. The mass spectra were fairly similar for all examined MOUDI stages as illustrated in Fig. S2 in the ESI section.† However, there was a small but reproducible

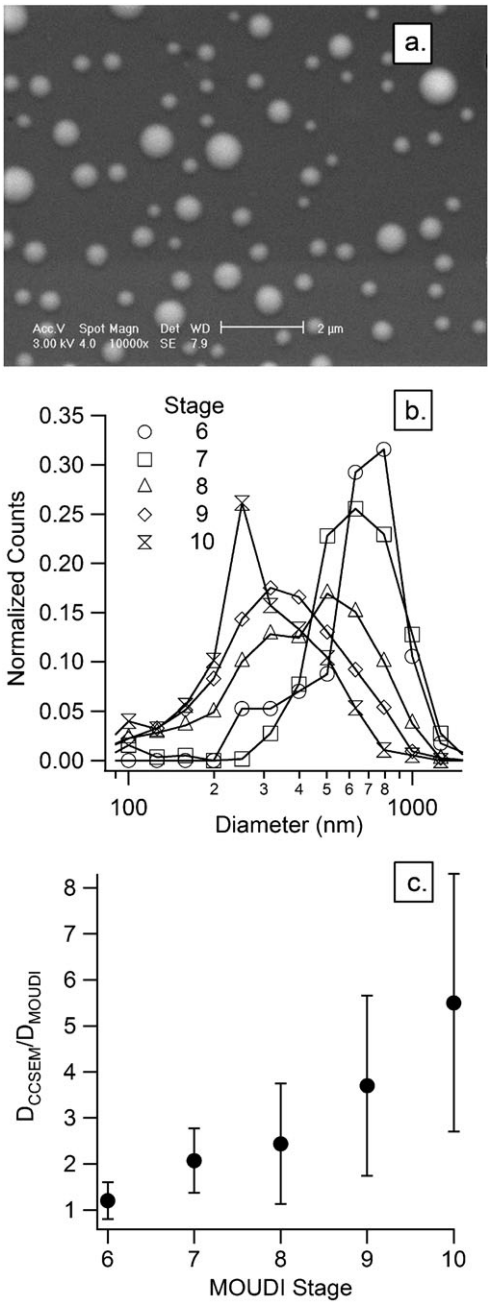

Fig. 3 (a) Representative CCSEM image of particles collected on Stage 7 of MOUDI from the dark reaction of D-limonene and ozone (scale bar = 2μm). (b) Distribution of the apparent particle sizes for stages 6-10 as measured by CCSEM. (c) Ratio of the average apparent size to the MOUDI cut-off diameter plotted against the MOUDI stage. Error bars correspond to one standard deviation.

difference between samples collected after 10 min and 90 min of reaction. Specifically, the oxidation state of molecules appeared to increase slightly with time. To better illustrate this point, Fig. 4 shows the average O : C and H : C ratios calculated from eqn (8) and (9), respectively, for stages 7 through 10. After 90 min of reaction, the H : C ratio did not change within experimental uncertainties, whereas the O : C increased from 0.43 to 0.46.

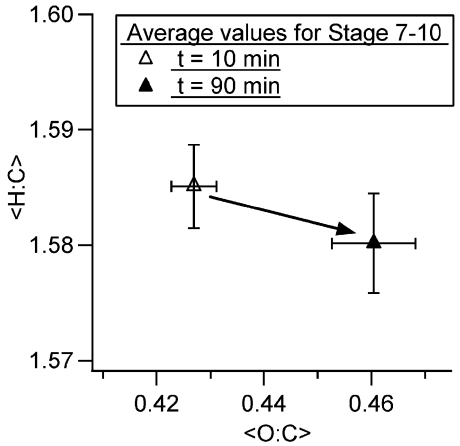

Fig. 4 Average H : C and O : C values calculated for stages 7 through 10. Data for two MOUDI samples, 10 min and 90 min after the injection of limonene are plotted. Error bars correspond to one standard deviation for the corresponding ratios.

To examine the observed evolution of the average chemical composition with better time resolution, we analyzed several batches of the DRUM impactor data. Weighted average O : C ratios, H : C ratios and DBE values were computed from eqns (8)–(10) for each spectrum. Fig. 5 shows a representative result, with these values plotted as a function of the reaction time for four separate subsets of the SOA constituents corresponding to the monomeric (150–300 m/z), dimeric (300–500 m/z), trimeric (500–700 m/z) and tetrameric (700–1000 m/z) regions in the mass spectra. The average DBE values increase in this order, as can be expected from Fig. 2. However, within a given subset of products, they do not significantly change with time. The average O : C ratios systematically increase with the reaction time and tend to level off after ~1 h, with the typical final values of ~0.44 for the monomer and dimer regions and ~0.46 for the trimer and tetramer region. In all the other data sets we examined, products with larger molecular weights similarly appeared to have slightly higher average O : C ratios. The average H : C ratio has a much smaller spread than the O : C ratio and shows no significant time dependence.

Similar plots were constructed for SOA samples prepared under different relative humidity and UV radiation levels (Fig. 6). The reaction conditions include: (i) dark reaction in dry air; (ii) reaction in dry air in the presence of UV radiation; (iii) reaction in dry air with the UV lamps turned on 30 min after mixing the reagents; (iv) dark reaction at ~15% RH; (iv) dark reaction at ~40%RH. Additionally, the O : C and H : C ratios calculated from the MOUDI samples (stages 7–10 combined) are included for comparison. For simplicity, the H : C and O : C ratios are not differentiated by the region of the mass spectra as in Fig. 5, but are computed for the entire set of assigned SOA constituents. The average DBE values for all reaction conditions are nearly identical to those for the dark reaction, and have no significant time dependence; they are not shown in Fig. 6. The slow increase in the O : C ratio was observed for all reaction conditions, with an excellent agreement between the MOUDI samples and DRUM rotating strip impactor samples. Within the experimental uncertainties, the H : C ratios were constant

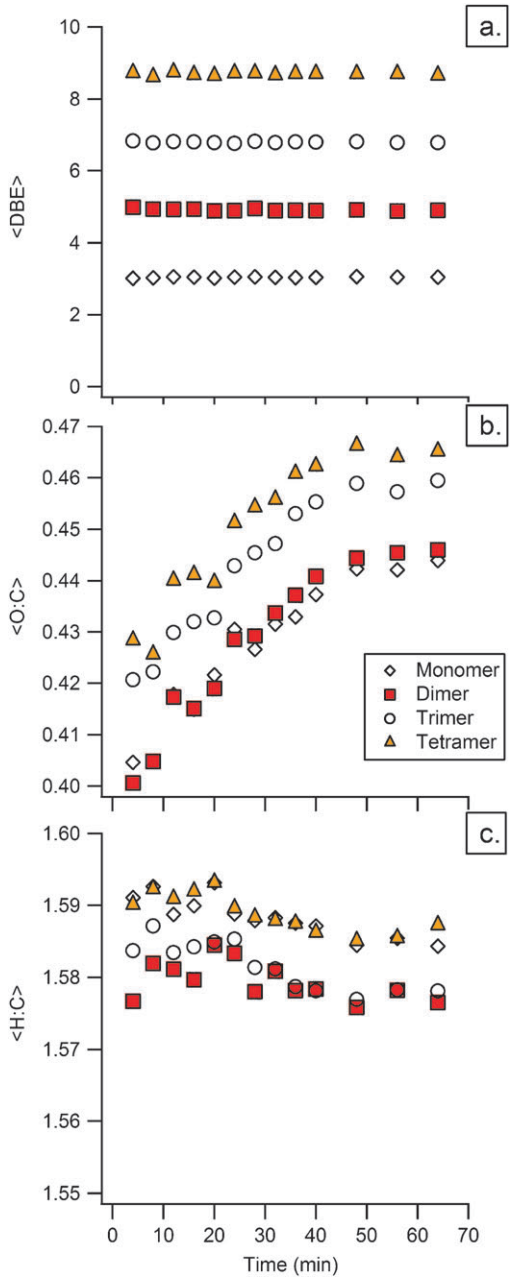

Fig. 5 Averaged properties of SOA collected during dark reaction of D-limonene and ozone using a DRUM impactor *vs.* reaction time and region of the mass spectra: (a) average DBE; (b) average O : C; (c) average H : C.

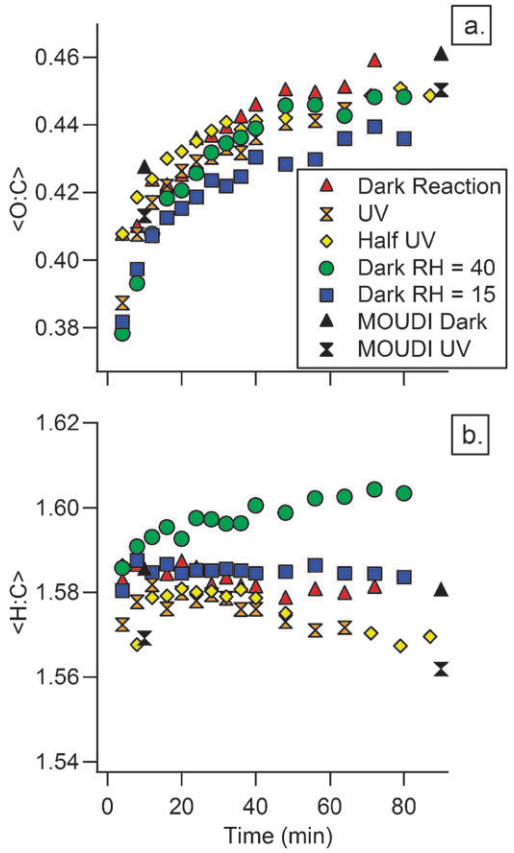

Fig. 6 Time dependence for (a) average O : C and (b) average H : C ratios under different conditions in the reaction chamber. Black symbols result from MOUDI samples and colored symbols result from DRUM rotating strip impactor samples. Reaction conditions include: dark—no radiation, dry air; UV-radiation is on during entire reaction, dry air; half UV-radiation turned on after 30 min of reaction time, dry air; RH = humidified air, no UV radiation.

under different reaction conditions. Only the high RH experiments showed measurable increase in the H : C ratio.

Discussion

1 Molecular composition of limonene/O_3 SOA

The observed DBE values for all monomeric SOA products fall between 2 and 4. Limonene itself has a DBE of 3, corresponding to its two C=C double bonds and one ring. The most prominent first generation products of limonene ozonolysis, such as endo-ozonide, limonic acid, limononic acid, limonalic acid, 7-hydroxy-limononaldehyde, 7-hydroxy-limononic acid, and limononaldehyde also have a DBE of 3 (structures of these products are shown in Fig. S4 of the ESI section†). Although ozone destroys the limonene's endocyclic double bond and opens up its six-membered ring, reducing DBE by 2, this is compensated by the formation of two new C=O bonds (*e.g.*, carbonyl and carboxyl) or two new rings in the case of the endo-ozonide. Subsequent oxidation of the exocyclic double bond into a carbonyl maintains the DBE value at 3 in products like keto-limononaldehyde or keto-limononic acid. Formation of monomeric products with DBE of 2 and 4 requires more complicated chemistry involving multiple isomerization and/or decomposition processes in alkoxy radicals formed from the decomposition of the Criegee intermediates.[18] Selected examples of the first generation products with DBE of 2 and 4 are also included in Fig. S4 of the ESI section.†

There is a clear tendency for the DBE value to increase with the molecular weight of the SOA compounds (Fig. 2). The most common DBE values for the monomeric, dimeric, trimeric, and tetrameric products are 3, 5, 7, and 9, respectively (Fig. 5). This increase by two DBE units is consistent with oligomer formation occurring by reactions

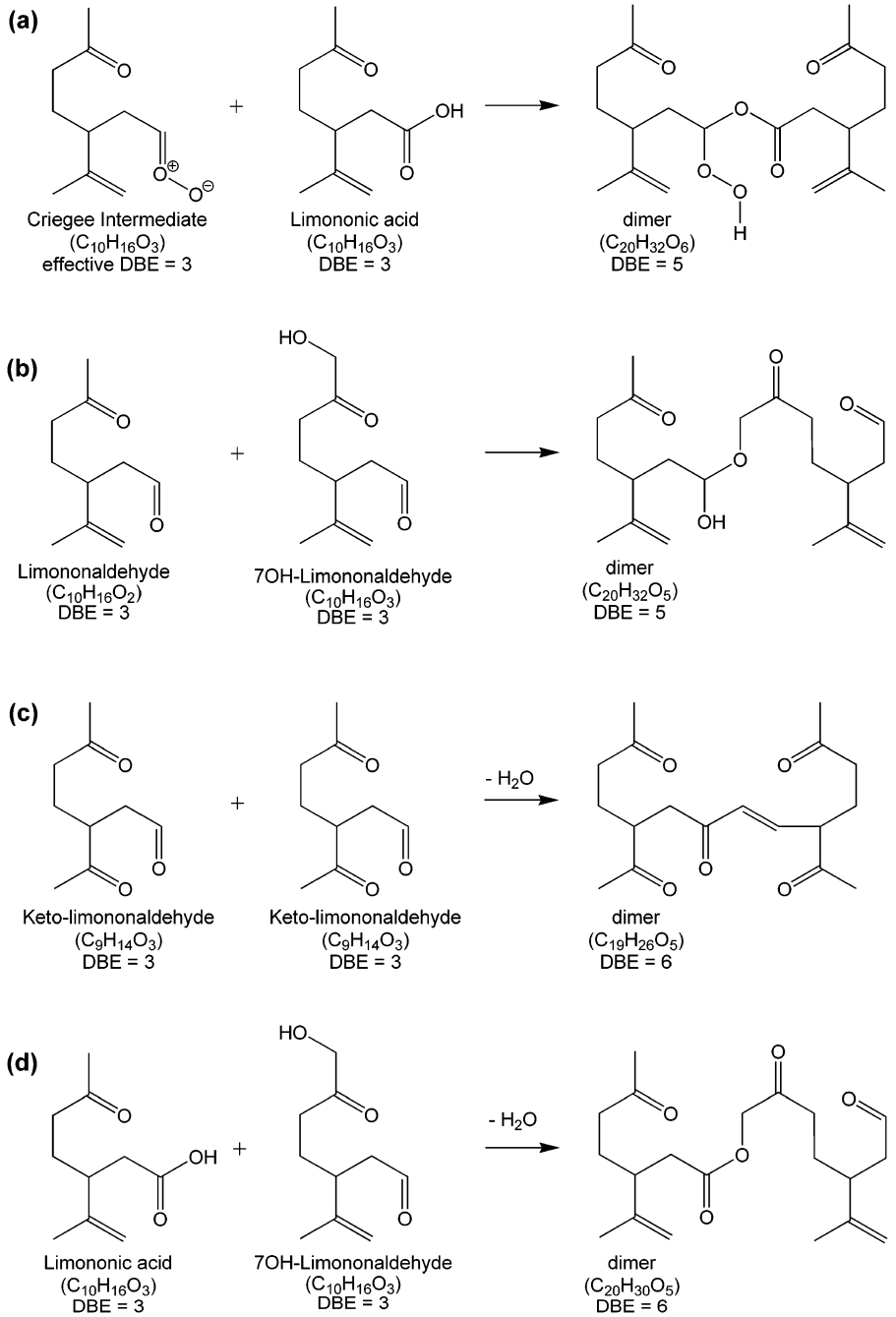

Fig. 7 Growth of DBE in different oligomerization reactions. (a) reaction between a Criegee intermediate and an acid or alcohol; (b) hemiacetal formation from an aldehyde and an alcohol; (c) aldol condensation involving two aldehydes; (d) esterification reaction between a carboxylic acid and an alcohol. Mechanisms (a) and (b), which increase DBE by 2 per oligomerization step, are more consistent with the trend shown in Fig. 2.

between one of the first generation products (typical DBE = 3) and a Criegee intermediate formed in the initial attack of ozone on limonene. Both Criegee intermediates resulting from an attack on the endocyclic double bond have an effective DBE of 3, which corresponds to one remaining C=C double bond, one carbonyl group, and one carbonyl oxide group. Fig. 7a shows the formation of a DBE = 5 organic peroxide in reaction between limononic acid and one of the Criegee intermediates. This mechanism of oligomerization becomes operative already at the very early stages of ozonolysis.[7] As evidenced by the data in Figs. 1, 2 and 5, oligomers were found in samples collected only four minutes into the reaction and throughout the subsequent reaction, regardless of the particle size.

Another mechanism that increases DBE by 2 in each oligomerization step involves formation of hemiacetals through reactions of alcohols with aldehydes and ketones. Fig. 7b shows an example involving a reaction between two common limonene ozonolysis products, limononaldehyde (DBE = 3) and 7-hydroxy-limononaldehyde (DBE = 3).

Because the aldehyde group is destroyed during this reaction, DBE of the resulting dimer is 5. Formation of hemiacetals in reactions of SOA constituents with methanol is quite efficient when methanol is used as the SOA extraction solvent.[45] Presumably, intramolecular hemiacetal formation reactions can also occur in the SOA matrix or/and in SOA extracted in acetonitrile, contributing to the appearance of oligomeric species.

Condensation reactions such as aldol condensation and esterification have also been proposed as possible oligomerization mechanisms in SOA.[19,46] Unlike the Criegee intermediate reaction and hemiacetal formation considered above, DBE is additive in condensation reactions. For example, the product of an aldol condensation of keto-limononaldehyde (DBE = 3) with itself has a DBE of 6 (Fig. 7c). The esterification product produced from limononic acid (DBE = 3) and 7-hydroxy-limononaldehyde (DBE = 3) also has a DBE of 6 (Fig. 7d). If condensation reactions were the major oligomerization pathway, we would expect the DBE to increase by 3 on every step from monomers to dimers, trimers, *etc*. Therefore, the observed increase in DBE by 2 units (Fig. 2) suggests that oligomer formation *via* condensation reactions does not play an important role under the experimental conditions used in this study.

The majority of the observed SOA constituents appear to represent oxygen-rich aliphatic compounds. The aromaticity index (AI) values calculated form eqn (2) for the compounds forming the main cluster of points in the VK plot in Fig. 1 are all negative, which is consistent with the lack of aromatic rings in the molecules. However, there is a small group of compounds with considerably lower H : C values and positive AI values. They appear as "outliers" in the VK plots, and are especially easy to see in Fig. 1 and 2 as an isolated group of points with high DBE values. The calculated AI values for these compounds start to approach the AI = 0.5 threshold for the existence of aromatic structures. These compounds were found in nearly every mass spectrum, regardless of reaction time or particle size. They may arise from a cyclization of certain polyketide-like SOA constituents, which create aromatic rings separated by aliphatic carbons. With the exceptions of reactions carried out under unrealistically acidic conditions,[47] aromatic species have not been previously reported amongst products of ozonolysis of limonene or other monoterpenes. This chemical pathway certainly warrants further investigation as the presence of aromatic structures is likely to have a major effect on the optical (light absorbing) and chemical properties of SOA.

2 Particle size dependence of SOA composition

The general appearance of the mass spectra from different MOUDI stages (see Fig. S2 in the ESI section†) is similar for all size fractions suggesting that the chemical composition of SOA generated from the reaction of limonene and ozone is not especially sensitive to the particle size. Subtle changes in the relative peak intensities of monomer, dimer, trimer, and tetramer regions possibly originate from matrix effects in the ESI ionization. At low concentrations (below $\sim 10^{-6}$ M), the ion current is proportional to the concentrations of analytes, whereas at high concentrations (above $\sim 10^{-4}$ M) the ion current saturates.[39] At these high concentrations, surface-active analytes are expected to out-compete polar analytes for the limited excess charge.[37] With the amount of SOA material collected on each MOUDI stage ($\sim$ 30 μg), the effective overall concentration of SOA constituents was $\sim 10^{-4}$ M (assuming an effective molecular weight of 300 g mol^{-1}). Under these conditions, the higher molecular weight species in SOA can be artificially enhanced in intensity. This enhancement is clearly visible in the mass spectrum for MOUDI stage 9 (Fig. S2 in the ESI section†) which typically collected the largest amount of SOA material.

The average values of O : C and H : C ratios and the general appearance of the VK plots are nearly identical for all size fractions (see Fig. S5 in the ESI section). We attribute this to a prompt consumption of limonene and particle growth early in the reaction, before the first MOUDI sample was collected. The experiments described here were carried out with $\sim$1 ppm level of the initial ozone and limonene mixing ratios, with ozone being in a slight excess. The reaction rate constant between ozone and limonene of 2×10^{-16} cm^3 molec^{-1} s^{-1} translates into a reaction half-time of $\sim$3 min. The involatile fraction of the first generation products should therefore all condense into SOA within minutes after the limonene addition. Indeed, in all the experiments the particle mass-concentration and particle size, as measured by the SMPS (representative data are shown in Fig. S1†), increased the fastest during the first ten minutes after mixing the reagents. After that, the particle size grew slowly due to coagulation processes and particle mass concentration decreased slowly due to the wall loss. Therefore, both large particles that grew by coagulation and small particles that have not yet coagulated should contain more or less the same set of condensable organics.

3 Time dependence of SOA composition

Once particles are formed, the SOA constituents can participate in the following types of aging processes: (i) further oxidation of the initial products by the residual ozone, both in the gas and particle phase; (ii) photolysis by UV radiation; (iii) various reactions between the condensed SOA constituents; (iv) uptake of and reactions with H_2O vapor; (v) reactive uptake of gas-phase organic species, such as small aldehydes. Because there was a delay between collecting samples and taking their mass spectra, we cannot expect to be equally sensitive to all of these aging processes. MOUDI samples were collected twice during the reaction; the samples were promptly processed after that. The oxidation by ozone, UV photolysis, and reactive uptake of VOCs by the SOA particles ceased more or less immediately after the collection. However, the particles could still react with the H_2O vapor in the laboratory air ($\sim$20% RH), and any conceivable condensed-phase reactions between the SOA constituents (cross-esterification, acetal formation, *etc*.) likely continued on the MOUDI substrate with the same rate they were occurring in the chamber. The DRUM impactor collected the particles continuously throughout the reaction. The particles deposited on the strip remained exposed to some levels of the residual

ozone, humidity and VOCs carried with the sampling flow. All these factors could potentially suppress the time dependence of chamber processes. For example, if the only aging process taking place were slow oligomerization inside the particles, and all collected samples were then extracted and analyzed simultaneously, we would not expect to see significant changes in the mass spectra because the overall age of the particles, in the chamber and on the substrate, were the same.

Despite these limitations, several interesting trends emerged in the time-dependent mass spectra (Fig. 4–6). The particles collected in the first few minutes of reaction already had relatively high oxidation levels as measured by the average O : C ratio in the products (Fig. 5 and 6). The O : C ratio reached ~95% of its final level by the first 4 minutes and the remaining ~5% of O : C increase took almost an hour. At the same time there were no significant changes in the average DBE values and H : C ratios (Fig. 5). We suspect that these changes were due to a slow oxidation of the remaining exocyclic C=C double bonds by the residual ozone. Slow conversion of aldehydes into carboxylic acids by the residual ozone[48] or by organic peroxides present in the SOA could also contribute to the observed growth in the O : C ratio.

More information about the mechanism can be inferred from the time dependence of the relative abundances from homologous families of products with the same number of carbon and hydrogen atoms, but differing in the number of oxygen atoms. Fig. 8 shows the time evolution for two representative monomeric and dimeric families of products, $C_{10}H_{16}O_{x=2-6}$ and $C_{19}H_{30}O_{x=4-12}$. The dashed lines have been included to guide the eye, by following the general trend of each peak. It can be seen that the compounds with the lower oxygen content (smaller x) decrease with time, compounds with the larger oxygen content (larger x) increase with time, while the ones in the middle stay relatively constant. When averaged over the large number of such families of compounds present in limonene SOA, the net result is the slow increase in the O : C ratio. The characteristic reaction time in Fig. 8 appears to be on the order of ~30 min. If we assume ~1 ppm residual O_3, and adopt an Ostwald coefficient of ~2 for solubility of ozone in the limonene/O_3 material (typical value for polar organic solvents)[49] we obtain $k \sim 10^3$–10^4 L mol^{-1} s^{-1} for the effective rate constant between the dissolved ozone and SOA constituents. This value is similar to ozone-alkene rate constants in liquid phase.[50] It is two to three orders of magnitude larger than typical ozone-aldehyde rate constants. We therefore conclude that the major mechanism of the O : C increase was ozonolysis of the exocyclic C=C double bonds in the first generation SOA products.

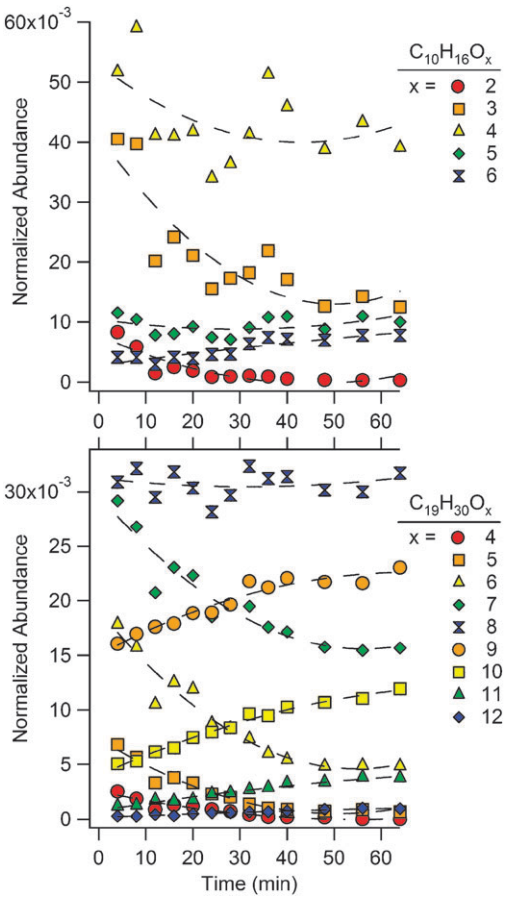

Fig. 8 Normalized peak intensities for the $C_{10}H_{16}O_x$ and $C_{19}H_{30}O_x$ families of products as a function of time during a dark reaction of limonene and ozone. Dashed lines represent polynomial fits to data as guides.

4 Effects of relative humidity and UV radiation

Presence of the UV radiation in the reaction chamber had rather insignificant effect on the molecular composition of limonene/O_3 SOA, as evidenced by the insensitivity of the average O : C and H : C ratios to UV (Fig. 6). Under the present experimental conditions, the changes in the observed mass spectra were relatively subtle. The UV radiation caused a slight redistribution in the relative peak intensities; it also generated some additional small peaks in the mass spectrum. Photodegradation of the SOA material by solar UV radiation is likely to take place on a time scales of hours or even days.[13,14] This is much slower than the time scales of the

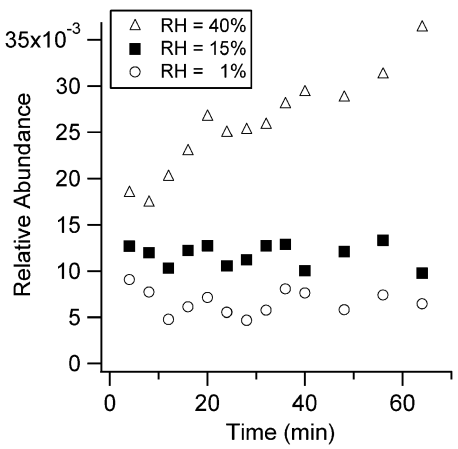

Fig. 9 Time dependence of the normalized abundance for m/z = 225.1096, $C_{10}H_{18}O_4Na^+$. The experiment was conducted in the dark with different initial%RH. The relative intensities are calculated by dividing the peak intensity by the sum of all peak intensities in the mass spectra.

competing processes: minutes for the formation of the first generation products; hours for the secondary oxidation chemistry.

The effect of the relative humidity was more pronounced. There was a clear shift of the relative peak intensities towards higher m/z values. Several peaks responded particularly strongly, with intensity changes taking place on a time scale of the order of one hour. For example, the peak at m/z 225.1096, $C_{10}H_{18}O_4Na^+$, increased significantly under humidified conditions (Fig. 9). Furthermore, this peak kept growing with time at 40% RH, possibly due to a slow hydration of the $C_{10}H_{16}O_3$ carbonyl compound resulting in its gem-diol form. The peak corresponding to $C_{10}H_{16}O_3$ decreased at higher%RH. Such hydration reactions are consistent with the small but reproducible H : C increase and with the faster growth in the O : C ratio with time (Fig. 6).

5 OM : OC ratios from HR-ESI-MS measurements

Using eqns (4)–(5) and replacing the molar fractions by the corresponding mass-spectral peak intensities, result in OM : OC ratio (organic mass to organic carbon mass) of $\sim$1.7 and OO : OC ratio (organic oxygen mass to organic carbon mass) of $\sim$0.6 for our limonene/O_3 SOA samples. The OM : OC value is close to the suggested value for the OM : OC ratio for the non-urban (2.1 $\pm$ 0.2) organic aerosols.[32] The OO : OC ratio is within the range of OO : OC ratios for water soluble species (0.4–2.0).[33] Both ratios provide a good match for the oligomeric organic compounds (OM : OC = 1.5–2.1; OO : OC = 0.4–1.0).[33,51] These observations suggest that the HR-ESI-MS techniques can provide reasonable estimates for the OM : OC and OO : OC ratios for the solvent extractable fraction of SOA. The HR-ESI-MS method obviously needs further validation and refinement. For example, our calculations assume equal detection sensitivities for all SOA constituents; the applicability of this approximation to SOA samples is yet to be tested. However, the small sample requirements of this method offer a significant advantage compared to more traditional techniques. In combination with an appropriate aerosol collector such as the DRUM impactor used in this work or with a particle-into-liquid sampler (PILS),[52] the HR-ESI-MS can potentially provide the OM : OC and OO : OC ratios with time resolution of several minutes.

6. Conclusions

We have applied the HR-ESI-MS methods to the molecular characterization of limonene/O_3 SOA samples as a function of the reaction time and conditions. The following conclusions can be drawn from this work.

(1) The HR-ESI-MS technique can be used to estimate the OM : OC ratio for the soluble fraction of SOA with a time resolution on the order of minutes. This method results in OM : OC $\sim$ 1.7 in the limonene/O_3 SOA.

(2) Molecules in limonene/O_3 SOA are highly oxidized. The average chemical formula for the SOA constituents is $CO_{0.45}H_{1.6}$. The average O : C ratio increases slowly as the aerosol ages, whereas H : C ratio stays roughly constant.

(3) An analysis of the distribution of double bond equivalency (DBE) factors and aromaticity index (AI) values suggest that limonene/O_3 SOA may contain a small fraction of aromatic species. These species are produced early in the ozone + limonene reaction by unknown chemical mechanisms.

(4) In agreement with previous research on SOA formation in ozonolysis of monoterpenes,[7,53,54] the limonene/O_3 SOA formation can be divided in two steps. The first generation products, including the oligomeric species, appear early in the reaction. The mechanism of oligomerization is consistent with fast reactions of Criegee intermediates with other products of ozonolysis. Further oxidation leading to the second generation products occurs in condensed phase on a much slower time scale. The dominant mechanism of this slow aging involves oxidation of the remaining double bonds in SOA constituents.

(5) In the presence of humidity, additional aging processes take place as a result of hydration reactions on a time scale of hours. The presence of UV radiation can lead to additional aging reactions that happen on even longer time scales.

Acknowledgements

The UCI group acknowledges support provided by the NSF Atmospheric Chemistry program, ATM-0831518 and also by the EMSI program, CHE-0431312. The PNNL group acknowledges support provided by the intramural research and development program of the W.R. Wiley Environmental Molecular Sciences Laboratory (EMSL) and funding by the Chemical Sciences Division, Office of Basic Energy Sciences of the US Department of Energy (DOE). APB acknowledges sponsorship provided by the DOE Global Change Education Program. This work was performed at EMSL, a national scientific user facility sponsored by OBER DOE and located at PNNL. PNNL is operated for US DOE by Battelle Memorial Institute under Contract No. DE-AC06-76RL0 1830.

References

1 C. Geron, R. Rasmussen, R. R. Arnts and A. Guenther, *Atmos. Environ.*, 2000, **34**, 1761–1781.
2 R. J. Griffin, D. R. Cocker, III, R. C. Flagan and J. H. Seinfeld, *J. Geophys. Res., [Atmos.]*, 1999, **104**, 3555–3567.
3 T. Hoffmann, J. R. Odum, F. Bowman, D. Collins, D. Klockow, R. C. Flagan and J. H. Seinfeld, *J. Atmos. Chem.*, 1997, **26**, 189–222.
4 J. Zhang, K. E. Huff Hartz, S. N. Pandis and N. M. Donahue, *J. Phys. Chem. A*, 2006, **110**, 11053–11063.
5 S. Leungsakul, M. Jaoui and R. M. Kamens, *Environ. Sci. Technol.*, 2005, **39**, 9583–9594.
6 J. K. Noejgaard, A. W. Noergaard and P. Wolkoff, *Atmos. Environ.*, 2007, **41**, 8345–8354.
7 K. J. Heaton, M. A. Dreyfus, S. Wang and M. V. Johnston, *Environ. Sci. Technol.*, 2007, **41**, 6129–6136.
8 M. Glasius, M. Duane and B. R. Larsen, *J. Chromatogr.*, 1999, **833**, 121–135.
9 M. Glasius, M. Lahaniati, A. Calogirou, D. Di Bella, N. R. Jensen, J. Hjorth, D. Kotzias and B. R. Larsen, *Environ. Sci. Technol.*, 2000, **34**, 1001–1010.
10 J. D. Hearn and G. D. Smith, *Int. J. Mass Spectrom.*, 2006, **258**, 95–103.
11 B. Warscheid and T. Hoffmann, *Rapid Commun. Mass Spectrom.*, 2001, **15**, 2259–2272.
12 B. Warscheid and T. Hoffmann, *Rapid Commun. Mass Spectrom.*, 2002, **16**, 496–504.
13 S. A. Mang, D. K. Henricksen, A. P. Bateman, M. P. S. Andersen, D. R. Blake and S. A. Nizkorodov, *J. Phys. Chem. A*, 2008, **112**, 8337–8344.

14 M. L. Walser, J. Park, A. L. Gomez, A. R. Russell and S. A. Nizkorodov, *J. Phys. Chem. A*, 2007, **111**, 1907–1913.
15 U. Baltensperger, M. Kalberer, J. Dommen, D. Paulsen, M. R. Alfarra, H. Coe, R. Fisseha, A. Gascho, M. Gysel, S. Nyeki, M. Sax, M. Steinbacher, A. S. H. Prevot, S. Sjogren, E. Weingartner and R. Zenobi, *Faraday Discuss.*, 2005, **130**, 265–278.
16 Y. Rudich, N. M. Donahue and T. F. Mentel, *Annu. Rev. Phys. Chem.*, 2007, **58**, 321–352.
17 A. Reinhardt, C. Emmenegger, B. Gerrits, C. Panse, J. Dommen, U. Baltensperger, R. Zenobi and M. Kalberer, *Anal. Chem.*, 2007, **79**, 4074–4082.
18 M. L. Walser, Y. Desyaterik, J. Laskin, A. Laskin and S. A. Nizkorodov, *Phys. Chem. Chem. Phys.*, 2008, **10**, 1009–1022.
19 M. P. Tolocka, M. Jang, J. M. Ginter, F. J. Cox, R. M. Kamens and M. V. Johnston, *Environ. Sci. Technol.*, 2004, **38**, 1428–1434.
20 J. S. Smith, A. Laskin and J. Laskin, *Anal. Chem.*, 2009, **81**, 1512–1521.
21 A. Laskin, J. S. Smith and J. Laskin, *Environ. Sci. Technol.*, 2009, **43**, 3764–3771.
22 A. S. Wozniak, J. E. Bauer, R. L. Sleighter, R. M. Dickhut and P. G. Hatcher, *Atmos. Chem. Phys.*, 2008, **8**, 5099–5111.
23 A. Calogirou, B. R. Larsen and D. Kotzias, *Atmos. Environ.*, 1999, **33**, 1423–1439.
24 A. Lee, A. H. Goldstein, M. D. Keywood, S. Gao, V. Varutbangkul, R. Bahreini, N. L. Ng, R. C. Flagan and J. H. Seinfeld, *J. Geophys. Res., [Atmos.]*, 2006, **111**, D07302, DOI: 10.1029/2005JD006437.
25 A. Laskin, J. P. Cowin and M. J. Iedema, *J. Electron Spectrosc. Relat. Phenom.*, 2006, **150**, 260–274.
26 T. A. Cahill and P. Wakabayashi, in *Advances in Chemistry Series Measurement: Challenges in Atmospheric Chemistry*, 1993, vol. 232, pp. 211–228.
27 S. Kim, R. W. Kramer and P. G. Hatcher, *Anal. Chem.*, 2003, **75**, 5336–5344.
28 Z. Wu, R. P. Rodgers and A. G. Marshall, *Anal. Chem.*, 2004, **76**, 2511–2516.
29 C. A. Hughey, C. L. Hendrickson, R. P. Rodgers, A. G. Marshall and K. Qian, *Anal. Chem.*, 2001, **73**, 4676–4681.
30 J. Meija, *Anal. Bioanalyt. Chem.*, 2006, **385**, 486–499.
31 B. P. Koch and T. Dittmar, *Rapid Commun. Mass Spectrom.*, 2006, **20**, 926–932.
32 B. J. Turpin and H.-J. Lim, *Aerosol Sci. Technol.*, 2001, **35**, 602–610.
33 Y. Pang, B. Turpin and L. Gundel, *Aerosol Sci. Technol.*, 2006, **40**, 128–133.
34 A. C. Aiken, P. F. DeCarlo, J. H. Kroll, D. R. Worsnop, J. A. Huffman, K. S. Docherty, I. M. Ulbrich, C. Mohr, J. R. Kimmel, D. Sueper, Y. Sun, Q. Zhang, A. Trimborn, M. Northway, P. J. Ziemann, M. R. Canagaratna, T. B. Onasch, M. R. Alfarra, A. S. H. Prevot, J. Dommen, J. Duplissy, A. Metzger, U. Baltensperger and J. L. Jimenez, *Environ. Sci. Technol.*, 2008, **42**, 4478–4485.
35 K. E. Altieri, S. P. Seitzinger, A. G. Carlton, B. J. Turpin, G. C. Klein and A. G. Marshall, *Atmos. Environ.*, 2008, **42**, 1476–1490.
36 M. J. Perri, S. Seitzinger and B. J. Turpin, *Atmos. Environ.*, 2009, **43**, 1487–1497.
37 N. B. Cech and C. G. Enke, *Mass Spectrom. Rev.*, 2001, **20**, 362–387.
38 P. Kebarle, *J. Mass Spectrom.*, 2000, **35**, 804–817.
39 C. Enke, *Anal. Chem.*, 1997, **69**, 4885–4893.
40 S. Gao, N. L. Ng, M. Keywood, V. Varutbangkul, R. Bahreini, A. Nenes, J. He, K. Y. Yoo, J. L. Beauchamp, R. P. Hodyss, R. C. Flagan and J. H. Seinfeld, *Environ. Sci. Technol.*, 2004, **38**, 6582–6589.
41 S. Gao, M. Keywood, N. L. Ng, J. Surratt, V. Varutbangkul, R. Bahreini, R. C. Flagan and J. H. Seinfeld, *J. Phys. Chem. A*, 2004, **108**, 10147–10164.
42 D. S. Gross, M. E. Gaelli, M. Kalberer, A. S. H. Prevot, J. Dommen, M. R. Alfarra, J. Duplissy, K. Gaeggeler, A. Gascho, A. Metzger and U. Baltensperger, *Anal. Chem.*, 2006, **78**, 2130–2137.
43 Y. Liu, J. P. Cain, H. Wang and A. Laskin, *J. Phys. Chem. A*, 2007, **111**, 10026–10043.
44 Y. Liu, E. R. Gibson, J. P. Cain, H. Wang, V. H. Grassian and A. Laskin, *J. Phys. Chem. A*, 2008, **112**, 1561–1571.
45 A. P. Bateman, M. L. Walser, Y. Desyaterik, J. Laskin, A. Laskin and S. A. Nizkorodov, *Environ. Sci. Technol.*, 2008, **42**, 7341–7346.
46 Y. Iinuma, O. Boge, T. Gnauk and H. Herrmann, *Atmos. Environ.*, 2004, **38**, 761–773.
47 S. M. Kane, R. S. Timonen and M.-T. Leu, *J. Phys. Chem. A*, 1999, **103**, 9259–9265.
48 J. E. Shilling, S. M. King, M. Mochida, D. R. Worsnop and S. T. Martin, *J. Phys. Chem. A*, 2007, **111**, 3358–3368.
49 *Solubility Data Series, vol. 7: Oxygen and Ozone*, ed. R. Battino, Pergamon Press, New York, 1981.
50 J. Hoigne and H. Bader, *Water Res.*, 1983, **17**, 173–183.
51 M. Kalberer, D. Paulsen, M. Sax, M. Steinbacher, J. Dommen, A. S. H. Prevot, R. Fisseha, E. Weingartner, V. Frankevich, R. Zenobi and U. Baltensperger, *Science*, 2004, **303**, 1659–1662.
52 R. J. Weber, D. Orsini, Y. Daun, Y. N. Lee, P. J. Klotz and F. Brechtel, *Aerosol Sci. Technol.*, 2001, **35**, 718–727.
53 M. P. Tolocka, K. J. Heaton, M. A. Dreyfus, S. Wang, C. A. Zordan, T. D. Saul and M. V. Johnston, *Environ. Sci. Technol.*, 2006, **40**, 1843–1848.
54 N. L. Ng, J. H. Kroll, M. D. Keywood, R. Bahreini, V. Varutbangkul, R. C. Flagan, J. H. Seinfeld, A. Lee and A. H. Goldstein, *Environ. Sci. Technol.*, 2006, **40**, 2283–2297.

